Electrocatalysis manuscript No.
(will be inserted by the editor)

Spontaneous deposition of iridium onto nickel substrates for the oxygen evolution reaction

Sophia R. Mellsop · Alister Gardiner · Aaron T. Marshall

Received: date / Accepted: date

Abstract Spontaneous deposition of Ir onto Ni substrates was investigated as a method to produce electrocatalytic layers for the oxygen evolution reaction in 30% KOH solution. UV/Vis spectroscopy, cyclic voltammetry and other electrochemical methods are used to investigate the deposition process and the activity of the electrocatalytic coating towards the oxygen evolution reaction. From three solutions ($IrCl_3$+HCl, H_2IrCl_6+HCl, and H_2IrCl_6), H_2IrCl_6 is shown to give the most active and stable coating, with deposition times of 45 minutes at 60 °C enough to increase the activity of the Ni substrate for the oxygen evolution reaction. It is proposed that Ir deposition can occur via the reduction of the Ir precursor coupled to Ni oxidation, as well as the hydrolysis and localised precipitation of the Ir precursor due to the increase in surface pH during Ni dissolution.

Keywords Iridium oxide · Nickel oxide · Oxygen Evolution Reaction · Alkaline water electrolysis · Electrocatalysis

1 Introduction

To improve the energy efficiency of water electrolysers, electrocatalysts are used to decrease the overpotentials of the oxygen and hydrogen evolution reactions. These electrocatalysts must have high electrocatalytic activity, high

Sophia R. Mellsop
Department of Chemical and Process Engineering, University of Canterbury, Christchurch 8140, New Zealand

Alister Gardiner
Callaghan Innovation (Research) Limited, Christchurch 8144, New Zealand

Aaron T. Marshall
Department of Chemical and Process Engineering, University of Canterbury, Christchurch 8140, New Zealand
E-mail: aaron.marshall@canterbury.ac.nz

active surface areas, and be stable for long periods, while being inexpensive and easy to manipulate [1,2]. Iridium oxide is very active for the oxygen evolution reaction (OER) with Tafel slopes as low as 40 mV and overpotentials as low as 83 mV at 10 mA cm^{-2} [3–5]. However, as Ir is an expensive metal, normally thin coatings of iridium (or iridium oxide) on inert substrates are used as the active electrodes.

Spontaneous deposition is one approach whereby noble metals can be coated onto Ni substrates [6–10]. In this method, the noble metal precursor is reduced onto the surface of Ni substrate through the oxidation of the Ni to Ni^{2+} [6,7]. This approach has been used to produce Ir-Ni and Ru-Ni electrodes for the hydrogen evolution reaction (HER) [6–8,10], and RuO_2-Ni anodes for the OER [6]. Ir-Ni cathodes for the HER have also been successfully prduced via electrodepsoition of Ir onto Ni [11]. However despite the well-known activity of IrO_x for the OER, spontaneous deposition has not yet been investigated as a method to produce OER electrocatalysts. Importantly, $IrNiO_x$ core - shell nanoparticles were recently shown to be more active and more stable for OER than IrO_x supported on either carbon or doped-SnO_2 [12] and have been suggested to have higher intrinsic activity for OER compared to pure Ir electrocatalysts [13]. Similarly, others have shown that IrO_2/Ni anodes prepared by electrochemical deposition are more active than pure Ni substrates for the OER [14]. Here, spontaneous deposition of Ir onto Ni foil is investigated as a simple method to produce active Ir layers for the OER in concentrated KOH electrolytes. Specifically, the effect of the Ir precursor and deposition time on the activity of these electrodes is reported.

2 Experimental

1 cm^2 Ni foil substrates (Sigma-Aldrich $\geq$ 99.9%) were cleaned in acetone for 5 minutes, ultrasonicated in soapy water, and then thoroughly rinsed with deionised (18.2 MΩ) water. These clean foils were then etched in 1 M HCl solution with 5.25 g L^{-1} of hydrogen peroxide for 15 minutes and finally rinsed in deionised water. Contact with the Ni foil was achieved by spot welding a Ni wire (0.5 mm diameter) to the foil. The deposition process was performed immediately after substrate preparation to reduce the effects of self-passivation of the freshly etched Ni foil.

Spontaneous deposition was performed at 60°C for 30-120 minutes in one of three solutions: 0.001 M H_2IrCl_6 + 0.1 M HCl (Solution A), 0.001 M H_2IrCl_6 (Solution B), or 0.001 M $IrCl_3$ + 0.1 M HCl (Solution C). The precursor solutions were deaerated with 40 cm^3 min^{-1} Ar for at least 10 minutes prior to and during deposition [7,8,11,10]. After deposition, the Ir modified electrodes were rinsed in DI water then dried at 60°C for 1 hour prior to electrochemical characterisation.

Electrochemical testing was performed in a thermostatically controlled (25°C) PTFE cell with 30 wt% KOH electrolyte, a nickel foil (30 cm^2) counter electrode and a Hg/HgO/30 wt% KOH reference electrode. All potentials in

this work are given relative to the Hg/HgO/30 wt% KOH reference electrode unless otherwise stated, where $E_{\mathrm{Hg/HgO/30\%KOH}} = 0.933$ V *vs.* RHE [15]. Cyclic voltammetry and galvanostatic oxygen evolution were performed using a Gamry Instruments Reference 3000 potentiostat, and in all cases the ohmic resistance between the working and reference electrode was compensated (either using positive-feedback for the voltammetry or post-measurement for galvanostatic measurements) using the value determined by electrochemical impedance spectroscopy. Cyclic voltammetry was conducted both before and after 6 hours of galvanostatic oxygen evolution to assess the stability and changes to the electrochemical behaviour of the coated electrodes during oxygen evolution.

UV/Vis spectroscopy was performed on the precursor solutions using a Shimadzu multispec 1500 UV/Vis spectrometer in a quartz crystal curvette over the 200-800 nm range. To confirm that changes in the precursor solution was due to the deposition process itself and not just ageing of the precursor solutions [10], the absorbance of unused solutions was also measured in parallel with the solutions used in the deposition process.

3 Results and Discussion

3.1 Influence of the iridium precursor solution

While both $IrCl_3$ and H_2IrCl_6 solutions have been used for spontaneous deposition of Ir in previous literature [8,10], no direct comparison between these precursors has been reported and thus we began by investigating the influence of the Ir precursor. In some cases, HCl has been added to the precursor solution [7,16,10], and so three solutions were chosen for comparison: 0.001 M H_2IrCl_6 + 0.1 M HCl (Solution A), 0.001 M H_2IrCl_6 (Solution B), and 0.001 M $IrCl_3$ + 0.1 M HCl (Solution C).

Absorption spectra were recorded for the three solutions prior to use (Figure 1a), with the H_2IrCl_6 containing solutions exhibiting peaks (415, 432 and 488 nm) characteristic of the $[IrCl_6]^{2-}$ complex [17–20]. The UV/Vis spectra of solution A and B also have a very small peak at 360 nm which is most likely from $[IrCl_6]^{3-}$ which also has a peak at 415 nm [17]. While we cannot quantify the concentration of $[IrCl_6]^{3-}$ present in this solution, as the molar absorptivity of $[IrCl_6]^{3-}$ is about 30x less than $[IrCl_6]^{2-}$, it is likely that solution A and B contain more than trace amounts of $[IrCl_6]^{3-}$. In addition to the peaks attributed to $[IrCl_6]^{2-}$ and $[IrCl_6]^{3-}$, clear peaks are also observed at 305 and 580 nm. While these are also seen in the $[IrCl_6]^{2-}$ spectra reported previously [17,18], others have suggested that the peaks at 305 and 580 nm originate form $[Ir(OH)_6]^{2-}$ and Ir-O-Ir linkages respectively [21]. For solution C (prepared from $IrCl_3$), clear peaks at 327 and 390 nm and a small peak at 550 nm were observed, and as expected the overall absorbance of this solution was much lower than the solutions prepared from H_2IrCl_6 [22,23]. In this case,

the peak at 390 nm is assigned to $Ir(H_2O)_3Cl_3$ [18], and the peak at 327 nm is assigned to the hydrolysis product $[Ir(OH)_6]^{3-}$ [24]. Interestingly, others have suggested that ageing the precursor solution prior to use can greatly improve the deposition process [7,10,16], so it is worthwhile to note that the aged $IrCl_3$ solution reported elsewhere [10] has a spectrum which suggests that aged $IrCl_3$ solutions contained a mixture of $[IrCl_6]^{3-}$, $[IrCl_6]^{2-}$ and $[Ir(OH)_6]^{2-}$.

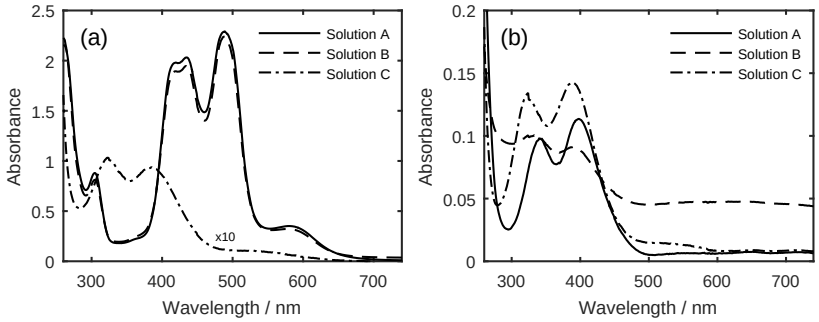

Fig. 1 UV visible spectra for the solutions prior to (a) and after deposition (c). Note that in (a) the absorbance of solution C is multiplied by 10

After 2 hours of deposition, significant changes to the solutions initially containing H_2IrCl_6 were observed, with the complete loss of the $[IrCl_6]^{2-}$ peaks and the development of a spectra similar to the initial $IrCl_3$ solution (Figure 1b). As the absorbance of solution B after deposition is significantly lower (relative to the background absorbance between 550 and 800 nm) than both the other precursor solutions, it is concluded that much more Ir is deposited onto the Ni substrate from solution B. For solutions A and B, the loss of $[IrCl_6]^{2-}$ supports the general proposal that the deposition process involves the reduction of $[IrCl_6]^{2-}$ to Ir:

$$[IrCl_6]^{2-} + 2\,Ni \rightleftharpoons Ir + 2\,Ni^{2+} + 6\,Cl^- \tag{1}$$

which is spontaneous as calculated from standard reduction potentials. The development of peaks at 330-340 nm and 390-400 nm suggests the formation of either $[IrCl_6]^{3-}$ (peaks at 360 and 415 nm [17]), $[Ir(OH)_6]^{3-}$ (320 nm [24]) or Ni^{2+} (394 nm [25]) via:

$$2\,[IrCl_6]^{2-} + Ni \rightleftharpoons 2\,[IrCl_6]^{3-} + Ni^{2+} \tag{2}$$

$$2\,[IrCl_6]^{2-} + 12\,H_2O + Ni \rightleftharpoons 2\,[Ir(OH)_6]^{3-} + Ni^{2+} + 12\,HCl \tag{3}$$

$$[IrCl_6]^{3-} + 6\,H_2O \rightleftharpoons [Ir(OH)_6]^{3-} + 6\,HCl \tag{4}$$

It is also possible that the formation of metallic iridium occurs from the reduction of the $[IrCl_6]^{3-}$ complex rather than directly from $[IrCl_6]^{2-}$:

$$2\,[IrCl_6]^{3-} + 3\,Ni \rightleftharpoons 2\,Ir + 3\,Ni^{2+} + 12\,Cl^- \tag{5}$$

The presence of Ni^{2+} which absorbs at 394 nm is difficult to confirm by UV/Vis spectroscopy as this absorbs at similar wavelengths to the various Ir species which are also present in the solution. Others have identified Ni^{2+} either directly by UV/Vis spectroscopy [6] or by forming the Ni-dimethylglyoxime complex [7] when depositing Ru onto Ni substrates, and as thermodynamics suggest that Ni oxidation will occur in the presence of either $[IrCl_6]^{2-}$ or $[IrCl_6]^{3-}$ it is very likely that the solutions after deposition will contain Ni^{2+}. For solution C, while very little difference in the UV/Vis spectra before and after deposition was observed, the increase in absorbance (particularly the peak at 390 nm relative to the peak at 327 nm), is most likely due to the presence of Ni^{2+} and may suggest that some Ir deposition has also occurred in this solution.

For solution B, it was observed that the background absorption (e.g. that between 550 and 800 nm) increased considerably during the deposition process, most likely due to the formation of IrO_x nanoparticles within the solution (which exhibit a broad absorption peak around 570-580 nm [21,24,26]). In some cases, a faint blue precipitate was observed in solution B after deposition which is likely to be IrO_x. This blue IrO_x precipitate was never found in solution B in absence of the Ni substrate, with no changes in the UV/Vis spectra of solution B observed over a 15 day period at room temperature. This precipitate was not observed in solution A and C, and suggests that this may occur due to the localised pH changes near the Ni substrate due to proton consumption:

$$2\,H^+ + Ni \rightleftharpoons H_2 + Ni^{2+} \tag{6}$$

As solution B did not contain HCl like solutions A and C, this proton consumption would increase the pH near the Ni surface, which would hydrolyse the $[IrCl_6]^{2-}$ or $[IrCl_6]^{3-}$, leading to IrO_x formation [21,24,26] and possibly IrO_x deposition directly onto the Ni substrate through a surface assisted nucleation process. This mechanism of oxide layer formation is very similar to cathodic deposition of oxides such as CoO_x [27], which uses cathodic hydrogen evolution to increase the surface pH thereby initiating localised oxide nucleation. To confirm that the hydrogen evolution reaction could be occurring in parallel with the Ir deposition process, the potential of the Ni substrate was measured and found to be around -0.22 to -0.2 V *vs.* AgAgCl (*i.e.* close to the hydrogen evolution potential). This supports our proposed mechanism of iridium oxide deposition via a localised pH increase brought about by the hydrogen evolution reaction, and the measured potential is consistent with that report by Duca et al. [10] where solution C was used. While this potential value and the observation of a blue IrO_2 precipitate is consistent with this proposed mechanism, the measured potential still allows direct deposition of metallic iridium to occur via reactions 1 or 5 and may be occurring in parallel with localised IrO_2 precipitation.

To confirm that the deposition procedure did modify the surface of the Ni substrates, cyclic voltammetry was performed before and after galvanostatic OER (Figure 2). For an uncoated Ni substrate, a set of peaks correspond-

ing to the $\alpha-Ni(OH)_2/\gamma-NiOOH$ transition are located at 0.41 (anodic) and 0.33 (cathodic) V along with a smaller anodic peak at 0.47 V which most believe corresponds to the $\beta-Ni(OH)_2/\beta-NiOOH$ transition [28]. These Ni redox peaks are seen on all the Ir modified electrodes indicating that if any Ir or IrO_2 layer had formed on these electrodes, it must be porous enough to allow electrolyte penetration to the substrate. This is consistent with other investigations where the Ni redox behaviour is observed by cyclic voltammetry after Ir deposition [8,14]. Based on the Pourbaix diagram for Ir [29], an anodic peak at approximately 0.09 V *vs.* Hg/HgO relating to the oxidation of Ir to IrO_2 is expected. Alternatively, for anodically formed IrO_x films, anodic solid-state redox peaks corresponding to the Ir^{3+}/Ir^{4+} and Ir^{4+}/Ir^{5+} transitions are expected to range from -0.17 to -0.03 V and from 0.14 to 0.26 V *vs.* Hg/HgO respectively. [30–33]. The corresponding cathodic solid-state redox peaks for the Ir^{4+}/Ir^{3+} and Ir^{5+}/Ir^{4+} transitions are expected to range from -0.3 to -0.11 V and from 0.10 to 0.12 V *vs.* Hg/HgO respectively. While any residual $[IrCl_6]^{3-}$ or $[IrCl_6]^{4-}$ species are unlikely to be stable in the concentrated KOH electrolyte used for the cyclic voltammetry measurements (these are both rapidly hydrolysed in KOH solutions), the redox potentials associated with either the $[IrCl_6]^{3-}$ /Ir or $[IrCl_6]^{3-}/[IrCl_6]^{4-}$ redox processes are expected at 0.76 and 0.86 V *vs.* HgHgO respectively and thus outside of the potential range used in these measurements.

Evidence for the Ir^{4+}/Ir^{3+} transition (within iridium oxide) is found for the electrode prepared by solution B, with a large cathodic feature starting at about 0 V (Figure 2B), although no corresponding anodic peak was found, possibly because of the lower potential limit used for these cyclic voltammograms. An additional set of peaks at 0.35 V (anodic) and 0.3 V (cathodic) not seen on the Ni substrate, were also found on the electrode prepared from solution B. While the redox behaviour of Ni can undergo significant changes during both cyclic voltammetry and OER [28], such peaks are not normally seen on pure Ni electrodes, suggesting that the Ir has indeed modified the Ni surface. One possibility is that Ir has been incorporated into the Ni oxyhydroxide film which is present on Ni substrates in KOH electrolyte, thereby altering the redox behaviour of the $Ni(OH)_2/NiOOH$ redox couple. It seems unlikely that this peak pair comes from the Ir^{4+}/Ir^{5+} transition which is reported at 0.14 to 0.26 V (anodic) and 0.10 to 0.12 V (cathodic) and upon close inspection of the voltammograms for this electrode, broad peaks at 0.26 V (anodic) and 0.18 V (cathodic) are found (Figure 7B shows are enlargement of the voltammograms to highlight these peaks) which are a better match to the reported potentials for the Ir^{4+}/Ir^{5+} transition. It is also noted that the background current related to the double layer charging at 0.1 V is significantly larger on the electrode prepared by solution B compared to the uncoated Ni substrate, suggesting that the deposition process has increased the electrode surface area. However, it is difficult to confirm that this increased current density is solely related to double layer charging effects as the potential range where the current density is constant is rather limited. It is also found that

the onset potential for the OER (defined as the potential at 1 mA cm^{-2}) is found to decrease following Ir deposition (0.64 → 0.5 V, Figure 2B) which is not surprising given that Ir is considerably more active than Ni for the OER. These findings lead to the conclusion that a stable Ir or IrO_2 porous layer was successfully deposited onto the Ni substrate when using solution B.

The voltammograms recorded at the electrodes prepared from solutions A and C are noticeably different to that prepared from solution B and are much more similar to the Ni voltammogram (Figures 2A and C). While the double layer charging current on these electrodes is larger relative to the uncoated Ni substrate, this current (measured at 0.1 V) is only about 25 % of the current measured at the electrode produced from solution B, suggesting that less Ir has been deposited, in agreement with the UV/Vis analysis. It is also possible that this increase in double layer charging is only due to roughening of the Ni substrate caused by Ni dissolution rather than Ir deposition, however for the electrodes produced from solutions A and C, additional redox peaks at 0.3 (anodic) and 0.12 (cathodic) V were observed in cyclic voltammetry measurements conducted immediately after Ir deposition (Fig 3). However was also found that the size of these peaks decrease during the initial cyclic voltammograms (Fig 3) and are completely absent from the electrodes after 6 hours of OER at 50 mA cm^{-2} indicating that the surface species which give these voltammetric peaks (possibly from the Ir^{4+}/Ir^{5+} transition) are not stable during cyclic voltammetry or OER. Furthermore, while the voltammograms measured just prior to the galvanostatic OER measurements have a lower onset potential for OER, after 6 hours of OER, unlike the electrode produced from solution B, this improvement is largely lost from the electrodes produced from solutions A and C.

In order to confirm the presence and stability of the Ir coating, SEM and EDS analysis was performed on the anodes after the initial cyclic voltammetry measurements and 6 hours of OER at 50 mA cm^{-2}. As expected the uncoated-etched Ni substrate showed a rather rough surface with the crystalline structure of the Ni clearly visible (Figure 4A). Following the deposition from solution B, a very thin film is observed to coat the Ni substrate (Figure 4B), with EDS analysis confirming that this layer is iridium. In some images, pores were visible through to the Ni substrate (confirm by EDS mapping) which accounts for the presence of the Ni redox peaks on the cyclic voltammograms. For the electrodes produced from solutions A and C, no evidence for any Ir deposits could be found by EDS mapping, confirming the suggestion that if these solutions did produce any Ir deposits, they were unstable during the cyclic voltammetry and 6 hours of oxygen evolution at 50 mA cm^{-2}. In previous work, both solutions B and C have been successfully used to produce stable coatings for the hydrogen evolution reaction [8,10], however in our investigation solution C failed to produce a stable layer. The most likely explanation for this is related to differences in the Ir species present in the precursor solutions due to precursor ageing [7]. In the investigation by Duca et al., their $IrCl_3$ was aged prior to deposition and importantly the UV/Vis spectra of their precursor solution [10] is markedly different to that found in

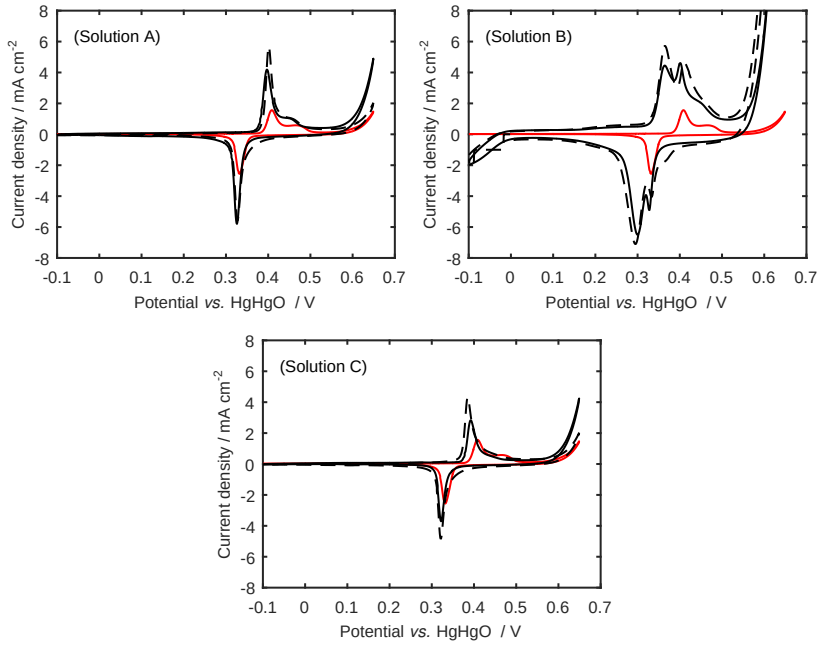

Fig. 2 Cyclic voltammograms before (solid lined) and after 6 hours of OER at 50 mA cm^{-2} (dashed line) on iridium coated nickel electrodes prepared from solutions A, B and C. For comparison, a typical voltammetry measured at an uncoated Ni substrate is also provide (red line)

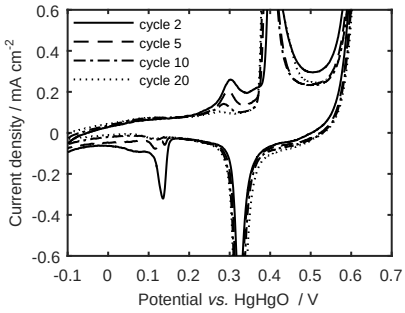

Fig. 3 Initial cyclic voltammograms of the iridium coated nickel electrode prepared from solutions C.

this work, with their aged $IrCl_3$ solution more similar to a fresh H_2IrCl_6 solution. Thus is seems likely the Ir species in the solutions used by Duca et al. [10] are actually quite different those in our solution C despite that fact that both solutions were prepared from $IrCl_3$ and HCl. It was also reported deposition of Ir from the aged solution C was very sensitive to the pre-treatment and etching of the Ni substrate [10] (the pre-treatment of the Ni in [10] involved boiling the Ni in 20% HCl) and thus, it may also be possible that both solution

A and C failed to produce a stable layer due to the pretreatment of the Ni in this work (although the SEM analysis does show that the Ni was well etched prior to the deposition).

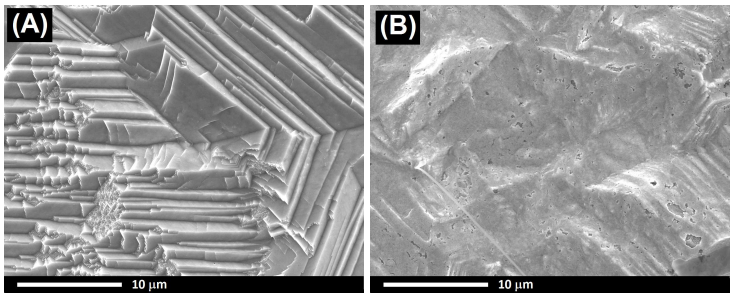

Fig. 4 SEM micrographs of (A) an uncoated Ni substrate and (B) a Ni substrate coated by Ir using solution B.

As only the electrode prepared from solution B was stable during cyclic voltammetry and OER at 50 mA cm^{-2}, the electrocatalytic activity of this electrode was compared with an uncoated Ni substrate (Figure 5). As discussed elsewhere, the activity of Ni for OER is strongly dependent on its pretreatment and can change dramatically when subjected to cyclic voltammetry prior to measuring the polarisation curve [34] or prolonged OER [27,28,35]. It has also been shown that the apparent electrocatalytic activity of Ni for the OER can depend on the scan direction used to measure puesdo-steady-state polarisation curves and periodic interruptions to galvanostatic OER [35]. This makes direct comparison to an uncoated Ni substrate quite difficult. Therefore in Figure 5, the polarisation curve for an uncoated Ni substrate recorded once a stable potential is reached at 50 mA cm^{-2}, the average potential during the 6 hour OER pretreatment at 50 mA cm^{-2} of the two uncoated Ni electrodes (prior to the polarisation curve measurements) is provided. While there is some uncertainty of the activity of uncoated Ni, it is clear that Ir deposition improves the anode for OER with the overpotential decreasing by at least 50 mV (over the current density range examined) compared with uncoated Ni. Given that the Ir deposition increased the surface area by approximately 10x (as judged by the double layer current measured at 0.1 V), the improvement in the OER performance could be simply due to surface area effects. However between 0.6 and 0.7 V, it is found that the current density increases by between 18x and 29x (at a given potential) and thus it appears that the Ir layer also has higher specific activity for the OER. It is also observed that the Tafel slope (an intrinsic measure of electrocatalytic activity) at low current densities is lower (40 *vs.* 70 mV) compared to uncoated Ni, although this lower Tafel slope is only found over a narrow potential window. For the electrodes prepared from solutions A and C, no clear difference in the OER activity compared to the uncoated Ni substrate was observed, which again suggested that these precursor solutions do not produce stable Ir layers by this method.

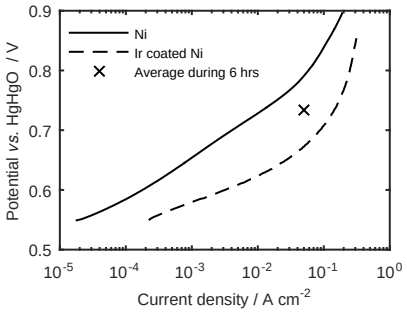

Fig. 5 Comparison of the electrocatalytic activity of an Ir coated Ni electrode (prepared from solution B) and an uncoated Ni electrode in 30 wt % KOH. The polarisation curves were measured between 0.55 and 1 V *vs.* HgHgO at 0.2 mV s^{-1} and corrected for the IR drop determined by EIS. The average potential during a 6 hour pretreatment at 50 mA cm^{-2} is also provided.

3.2 Deposition Time

To establish the optimum deposition time to produce an active Ir coating from solution, the deposition time was varied to between 30 and 120 minutes. Within 30 minutes, the UV/Vis absorbance peaks associated with the $[IrCl_6]^{2-}$ complex (432 and 488 nm) decreased by approximately 1 order of magnitude suggesting that the initial reaction of $[IrCl_6]^{2-}$ is quite rapid. For deposition times of 30-60 min, the $[Ir(OH)_6]^{2-}$ which was present in the fresh H_2IrCl_6 solution (peak at 305 nm) was still observed, however after 60 min this peak is lost suggesting that this undergoes further reactions such as reduction to $[Ir(OH)_6]^{3-}$ (peak at 330 nm) or hydrolysis/oxidation to IrO_x nanoparticles. We also note that for the samples at 30 and 45 min, a peak at 345 nm is found which we suggest is a convolution of the $[Ir(OH)_6]^{3-}$ and $[IrCl_6]^{3-}$ absorption peaks located at 330 and 360 nm respectively. It seems reasonable that both $[Ir(OH)_6]^{3-}$ and $[IrCl_6]^{3-}$ will be seen at short deposition times as these are probably intermediates formed from the reduction of the initial Ir species in precursor solution. Again it is likely that the peak located at 394 nm after 60 minutes is from Ni^{2+}, but it is not possible to confirm that this is present at shorter times due to the overlapping absorbance peaks from Ir species. As both hydrolysis and reduction products from $[IrCl_6]^{2-}$ are observed, we propose that the deposition process involves both the reduction of $[IrCl_6]^{2-}$ coupled with Ni oxidation, and the hydrolysis of Ir species due to localised pH changes, although further work is required to gain a complete understanding of the process.

For deposition times greater than 30 minutes, cyclic voltammetry clearly shows that electrodes exhibited both the $Ni(OH)_2$/NiOOH behaviour along with the additional redox peaks at 0.35 V (anodic) and 0.3 V (cathodic) as discussed previously (Figure 7a). The cathodic feature at -0.05 V and the broad redox peak couple at 0.26 V (anodic) and 0.18 V (cathodic shoulder) increases with deposition time (Figure 7b) as does the double layer charging current

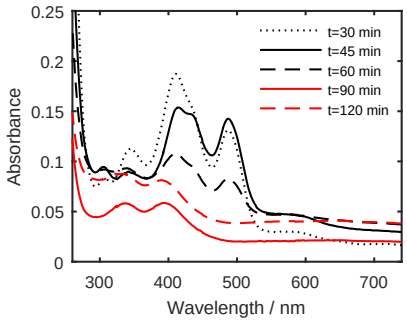

Fig. 6 UV visible spectra of solution B (0.001 M H_2IrCl_6) as a function of the deposition time.

density (Figure 7c), suggesting that longer deposition times lead to thicker Ir deposits. It is worth noting that the increased quantity of Ir in the layer does not decrease the current from the $Ni(OH)_2$/NiOOH transition, which shows that thicker Ir layers do not alter the accessibility of the electrolyte to the Ni substrate. The lack of features corresponding to a Ir layer at the 30 minute deposition time suggests that this time is too short to form a stable and electroactive Ir layer, most likely because the initial intermediates (e.g. $[Ir(OH)_6]^{3-}$ and $[IrCl_6]^{3-}$) have not had sufficient time to react further to form the Ir layer.

It is again clear that Ir deposition (for times greater than 30 minutes) improves the activity towards the OER relative to the uncoated Ni substrate (Figure 8). However despite the cyclic voltammetry suggesting that increasing the deposition time increases the quantity of Ir deposited on the Ni substrate, almost no difference in the electrocatalytic activity is found for deposition times of 45-120 minutes, suggesting that the activity is improved by a relatively small quantity of Ir. This is somewhat expected given that the OER is an electrocatalytic reaction which only occurs on the outer surface of the active Ir layer, and suggests that increasing the Ir deposition time increases the thickness of the Ir layer rather than generating more electrocatalytic surface area for the OER. Of course, the voltammetry did show an increase in the quantity of electrochemically active Ir, however it is well-known that unlike the OER, the solid-state redox transition in noble metal oxide films is not restricted to the outer-most surface of the oxide layer [36]. As with the cyclic voltammetry results, it is suggested that a deposition time of 30 minutes is insufficient to produce an active Ir layer on the Ni substrate, with this electrode exhibiting almost the same electrocatalytic activity as the uncoated Ni substrate (and actually even worse performance at high current densities). Interestingly, at 40-50 mAcm $^{-2}$, the Tafel slope of all the Ir modified electrodes increases from 40 mV to values much greater than 120 mV suggesting that the mechanism or rate limiting step for the OER changes at this current density. One possibility is that at these high current densities the active Ir sites become saturated with a reaction intermediate and thus a limiting current is approached. For

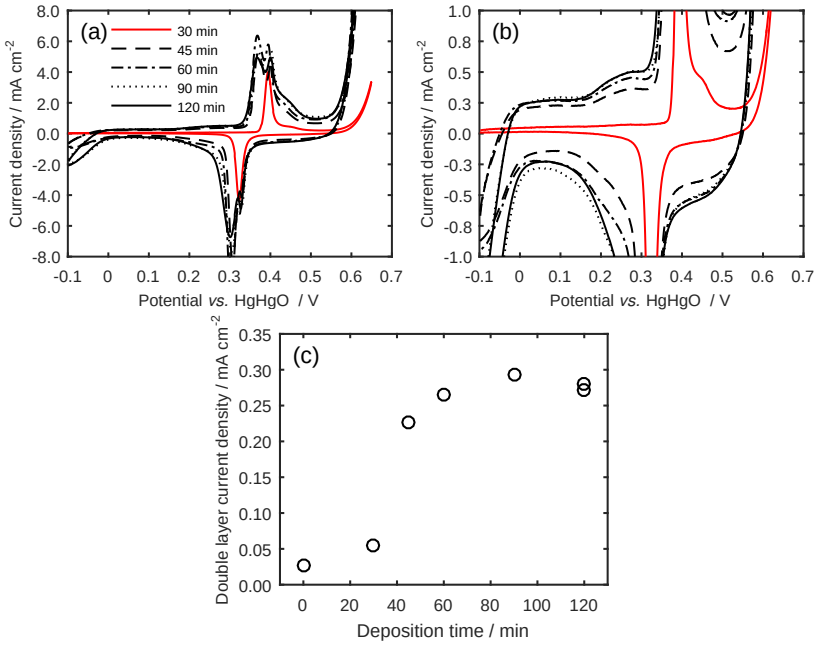

Fig. 7 Cyclic voltammograms (a) and (b) at 50 mV s^{-1} on electrodes with coatings deposited for 30-120 minutes. Double layer charging current density at 0.1 V vs deposition time (c)

example if the combination of adsorbed O to form molecular oxygen is rate limiting, and the surface coverage of O on the Ir sites $\rightarrow$ 1, the Tafel slope will approach infinity [37].To increase the current density further, the Ni must then begin to act as an electrocatalyst and the potential increases more rapidly with current density. This explanation is similar to that proposed by Duca *et al.* [10] when describing the kinetics of the hydrogen evolution reaction on Ir coated Ni prepared by spontaneous deposition.

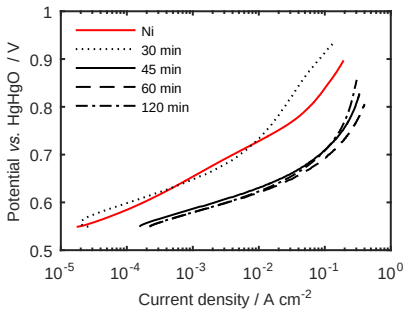

Fig. 8 Linear sweep voltammetry performed at 0.2 mV s^{-1} Ir modified Ni substrates prepared at different deposition times.

4 Conclusions

Spontaneous deposition can be utilized as a method for the production of thin Ir layers on Ni substrates for the electrocatalytic oxygen evolution reaction. The optimum solution for spontaneous deposition was found to be a dilute H_2IrCl_6 solution, which is believed to form the active layer on Ni through both reduction and hydrolysis / localised precipitation. Cyclic voltammetry revealed evidence of the active Ir coating and also confirmed that this layer is porous enough to allow electrolyte penetration to the underlying Ni substrate. At 60 °C, a deposition time of only 45 minutes is required to increase the activity of a Ni substrate towards the OER in 30 wt% KOH.

Acknowledgements Funding for this work has been provided under MSI Contract C08X1002

References

1. M. Momirlan and T. Veziroglu. Current status of hydrogen energy. *Renewable and sustainable energy reviews*, 6:141–179, 2002.
2. S. Trasatti. Electrocatalysis in the anodic evolution of oxygen and chlorine. *Electrochimica Acta*, 29:1503–1512, 1984.
3. M. Lyons and S. Floquet. Mechanism of oxygen reactions at porous oxide electrodes. Part 2 - Oxygen evolution at RuO_2, IrO_2 and $Ir_xRu_{1-x}O_2$ electrodes in aqueous acid and alkaline solution. *Physical Chemistry Chemical Physics*, 13(12):5314–5335, March 2011.
4. E. Guerrini, H. Chen, and S. Trasatti. Oxygen evolution on aged IrO_x/Ti electrodes in alkaline solutions. *Journal of Solid State Electrochemistry*, 11(7):939–945, May 2007.
5. H. Miao and D. Piron. Electrodeposition of Ni-transition alloys for the oxygen evolution reaction. *Journal of Applied Electrochemistry*, 21(1):55–59, January 1991.
6. H. Dumont, P. Los, A. Lasia, H. Ménard, and L. Brossard. Studies of the hydrogen evolution reaction on lanthanum phosphate-bonded composite nickel ruthenium electrodes in 1 M alkaline solutions. *Journal of Applied Electrochemistry*, 23(7):684–692, 1993.
7. I. Bianchi, E. Guerrini, and S. Trasatti. Electrocatalytic activation of Ni for H_2 evolution by spontaneous deposition of Ru. *Chemical Physics*, 319(1-3):192–199, 2005.
8. L. Vázquez-Gómez, S. Cattarin, P. Guerriero, and M. Musiani. Hydrogen evolution on porous Ni cathodes modified by spontaneous deposition of Ru or Ir. *Electrochimica Acta*, 53(28):8310–8318, November 2008.
9. E. Verlato, S. Cattarin, N. Comisso, A. Gambirasi, M. Musiani, and L. Vazquez-Gomez. Preparation of Pd-Modified Ni Foam Electrodes and Their Use as Anodes for the Oxidation of Alcohols in Basic Media. *Electrocatalysis*, 3(1):48–58, 2012.
10. M. Duca, E. Guerrini, A. Colombo, and S. Trasatti. Activation of Nickel for Hydrogen Evolution by Spontaneous Deposition of Iridium. *Electrocatalysis*, 4(4):338–345, December 2013.
11. L. Vázquez-Gómez, S. Cattarin, R. Gerbasi, P. Guerriero, and M. Musiani. Activation of porous Ni cathodes towards hydrogen evolution by electrodeposition of Ir nuclei. *Journal of Applied Electrochemistry*, 39(11):2165–2172, November 2009.
12. Hong Nhan Nong, Hyung-Suk Oh, Tobias Reier, Elena Willinger, Marc-Georg Willinger, Valeri Petkov, Detre Teschner, and Peter Strasser. Oxide-Supported $IrNiO_x$ CoreShell Particles as Efficient, Cost-Effective, and Stable Catalysts for Electrochemical Water Splitting. *Angewandte Chemie International Edition*, 54(10):2975–2979, 2015.
13. Hong Nhan Nong, Lin Gan, Elena Willinger, Detre Teschner, and Peter Strasser. IrO_x core-shell nanocatalysts for cost- and energy-efficient electrochemical water splitting. *Chemical Science*, 5(8):2955–2963, 2014.

14. Mirko Battaglia, Rosalinda Inguanta, Salvatore Piazza, and Carmelo Sunseri. Fabrication and characterization of nanostructured $NiIrO_2$ electrodes for water electrolysis. *International Journal of Hydrogen Energy*, 39(30):16797–16805, 2014.
15. R. A. Nickell, W. H. Zhu, R. U. Payne, D. R. Cahela, and B. J. Tatarchuk. Hg/HgO electrode and hydrogen evolution potentials in aqueous sodium hydroxide. *Journal of Power Sources*, 161(2):1217–1224, 2006.
16. W. Chrzanowski and A. Wieckowski. Ultrathin Films of Ruthenium on Low Index Platinum Single Crystal Surfaces: An Electrochemical Study. *Langmuir*, 13(22):5974–5978, October 1997.
17. Ingeborg A. Poulsen and Clifford S. Garner. A Thermodynamic and Kinetic Study of Hexachloro and Aquopentachloro Complexes of Iridium(III) in Aqueous Solutions. *Journal of the American Chemical Society*, 84(11):2032–2037, 1962.
18. James C. Chang and Clifford S. Garner. Kinetics of Aquation of Aquopentachloroiridate(III) and Chloride Anation of Diaquotetrachloroiridate(III) Anions. *Inorganic Chemistry*, 4(2):209–215, 1965.
19. I. Belova, T. Varlamova, B. Galyamov, Y. Roginskaya, R. Shifrina, S. Pruchenko, G. Kaplan, and M. Sevostyanov. The composition, structure and electronic properties of thermally prepared iridium dioxide films. *Mater. Chem. Phys.*, 20:39–64, 1988.
20. Y. Roginskaya and O. Morozova. The role of hydrated oxides in formation and structure of DSA-type oxide electrocatalysts. *Electrochim. Acta*, 40:817–822, 1995.
21. Yixin Zhao, Emil A. Hernandez-Pagan, Nella M. Vargas-Barbosa, Jennifer L. Dysart, and Thomas E. Mallouk. A High Yield Synthesis of Ligand-Free Iridium Oxide Nanoparticles with High Electrocatalytic Activity. *The Journal of Physical Chemistry Letters*, 2(5):402–406, 2011.
22. M. Schnippering, P. Unwin, J. Hult, T. Laurila, C. Kaminski, J. Langridge, R. Jones, M. Mazurenka, and S. Mackenzie. Evanescent wave broadband cavity enhanced absorption spectroscopy using supercontinuum radiation: A new probe of electrochemical processes. *Electrochemistry Communications*, 10(12):1827–1830, 2008.
23. Y. Roginskaya, O. Morozova, E. Loubnin, A. Popov, Y. Ulitina, V. Zhurov, S. Ivanov, and S. Trasatti. X-ray diffraction, transmission electron microscopy and X-ray photoelectron spectroscopic characterization of IrO_2 + Ta_2O_5 films. *Journal of the Chemical Society, Faraday Transactions*, 89(11):1707, 1993.
24. Di Xu, Peng Diao, Tao Jin, Qingyong Wu, Xiaofang Liu, Xin Guo, Hongyu Gong, Fan Li, Min Xiang, and Yu Ronghai. Iridium Oxide Nanoparticles and Iridium/Iridium Oxide Nanocomposites: Photochemical Fabrication and Application in Catalytic Reduction of 4-Nitrophenol. *ACS Applied Materials & Interfaces*, 7(30):16738–16749, 2015.
25. W. Liu, A. Migdisov, and A. Williams-Jones. The stability of aqueous nickel(II) chloride complexes in hydrothermal solutions: Results of UVVisible spectroscopic experiments. *Geochimica et Cosmochimica Acta*, 94:276 – 290, 2012.
26. M. Yagi, E. Tomita, and T. Kuwabara. Remarkably high activity of electrodeposited IrO_2 film for electrocatalytic water oxidation. *Journal of Electroanalytical Chemistry*, 579(1):83–88, 2005.
27. Sophia R. Mellsop, Alister Gardiner, and Aaron T. Marshall. Electrocatalytic Oxygen Evolution on Electrochemically Deposited Cobalt Oxide Films: Comparison with Thermally Deposited Films and Effect of Thermal Treatment. *Electrocatalysis*, pages 1–11, 2014.
28. Sophia R. Mellsop, Alister Gardiner, Bernt Johannessen, and Aaron T. Marshall. Structure and transformation of oxy-hydroxide films on Ni anodes below and above the oxygen evolution potential in alkaline electrolytes. *Electrochimica Acta*, 168:356–364, 2015.
29. M. Pourbaix. *Atlas of Electrochemical Equilibria in Aquesous Solutions*. Pergamon Press, New York, 1966.
30. Y. J. Chen, P. L. Taylor, and D. Scherson. Electrochemical and in situ optical studies of supported iridium oxide films in aqueous solutions. *Journal of the Electrochemical Society*, 156(1):14–21, 2009.
31. J. E. Baur and T. W. Spaine. Electrochemical deposition of iridium(IV) oxide from alkaline solutions of iridium(III) oxide. *Journal of Electroanalytical Chemistry*, 443(2):208–216, 1998.
32. M. Petit and V. Plichon. Anodic electrodeposition of iridium oxide films. *Journal of Electroanalytical Chemistry*, 444:247–252, 1998.

33. Y. Mo, I. Stefan, W. Cai, J. Dong, P. Carey, and D. Scherson. In situ iridium LIII-edge x-ray absorption and surface enhanced raman spectroscopy of electrodeposited iridium dioxide films in aqueous electrolytes. *Journal of Physical Chemistry B*, 106:3681–3686, 2002.
34. I. J. Godwin and M. E. G. Lyons. Enhanced oxygen evolution at hydrous nickel oxide electrodes via electrochemical ageing in alkaline solution. *Electrochemistry Communications*, 32:39–42, 2013.
35. Sophia R. Mellsop, Alister Gardiner, and Aaron T. Marshall. Electrocatalytic oxygen evolution on nickel oxy-hydroxide anodes: Improvement through rejuvenation. *Electrochimica Acta*, 180:501–506, 2015.
36. S. Ardizzone, G. Fregonara, and S. Trasatti. "Inner" and "Outer"' Active Surface of RuO_2 Electrodes. *Electrochimica Acta*, 35:263–267, 1990.
37. Aaron T. Marshall and Laurent Vaisson-Béthune. Avoid the quasi-equilibrium assumption when evaluating the electrocatalytic oxygen evolution reaction mechanism by Tafel slope analysis. *Electrochemistry Communications*, 61:23–26, 2015.